



Published in final edited form as:

*J Thorac Oncol.* 2022 December ; 17(12): 1375–1386. doi:10.1016/j.jtho.2022.08.008.

## A Knock-in Mouse Model of Thymoma with the *GTF2I* L424H Mutation

Yongfeng He<sup>a</sup>, In-Kyu Kim<sup>b</sup>, Jing Bian<sup>c</sup>, Alexander Polyzos<sup>a</sup>, Dafne Campigli Di Giammartino<sup>a</sup>, Yu-Wen Zhang<sup>b,†</sup>, Ji Luo<sup>d</sup>, Maria O. Hernandez<sup>e</sup>, Noemi Kedei<sup>e</sup>, Maggie Cam<sup>c</sup>, Alain C. Borczuk<sup>f,‡</sup>, Trevor Lee<sup>a</sup>, Yumin Han<sup>a</sup>, Elizabeth A. Conner<sup>g</sup>, Madeline Wong<sup>g</sup>, Desiree C. Tillo<sup>g</sup>, Shigeki Umemura<sup>b</sup>, Vincent Chen<sup>b</sup>, Lydia Ruan<sup>c</sup>, Jessica B. White<sup>h</sup>, Ileana C. Miranda<sup>i</sup>, Parirokh P. Awasthi<sup>j</sup>, Nasser K Altorki<sup>k</sup>, Prajan Divakar<sup>l</sup>, Olivier Elemento<sup>h</sup>, Effie Apostolou<sup>a</sup>, Giuseppe Giaccone<sup>a,b,\*</sup>

<sup>a</sup>Meyer Cancer Center, Weill Cornell Medicine, New York, NY10065, USA

<sup>b</sup>Department of Oncology, Lombardi Comprehensive Cancer Center, Georgetown University, Washington, DC20057, USA

<sup>c</sup>CCR Collaborative Bioinformatics Resource, Center for Cancer Research, National Cancer Institute, National Institutes of Health, Bethesda, MD 20892, USA

<sup>d</sup>Laboratory of Cancer Biology and Genetics, Center for Cancer Research, National Cancer Institute, Bethesda, MD 20892, USA

<sup>e</sup>Collaborative Protein Technology Resource, Office of Science and Technology, Center for Cancer Research, National Cancer Institute, National Institutes of Health, Bethesda, MD 20892, USA

<sup>f</sup>Department of Pathology, Sandra and Edward Meyer Cancer Center, Weill Cornell Medicine, New York, NY10065, USA

<sup>g</sup>CCR Genomics Core, National Cancer Institute, Bethesda, MD 20892, USA

<sup>h</sup>Caryl and Israel Englander Institute for Precision Medicine, New York-Presbyterian Hospital, Weill Cornell Medicine, New York, NY10065, USA

\*Corresponding author: Giuseppe Giaccone, gig4001@med.cornell.edu, 1300 York Ave. 6th floor, Rm A603C, New York, NY 10065.

†New address: Department of Cell Biology, University of Virginia, School of Medicine, Charlottesville, VA 22908, USA

‡New Address: Department of Pathology, Northwell Health, Greenvale, NY11548, USA

### Author Contributions:

**Yongfeng He:** Conceptualization, Investigation, Data curation, Formal analysis, Visualization and Original draft. **In-Kyu Kim:** Conceptualization and Methodology. **Jing Bian:** Methodology, Data curation and Formal analysis. **Alexander Polyzos:** Data curation and Formal analysis. **Dafne Campigli Di Giammartino:** Investigation. **Yuwen Zhang:** Methodology and Resources. **Ji Luo:** Methodology and Resources. **Maria O. Hernandez:** Methodology and Data curation. **Noemi Kedei:** Methodology and Data curation. **Maggie Cam:** Methodology and Data curation. **Alain C. Borczuk:** Investigation and validation. **Trevor Lee:** Investigation. **Yumin Han:** Investigation. **Elizabeth A. Conner:** Methodology and Data curation. **Madeline M.F. Wong:** Methodology and Data curation. **Desiree C. Tillo:** Methodology and Data curation. **Shigeki Umemura:** Investigation. **Vincent Chen:** Investigation. **Lydia Ruan:** Investigation. **Jessica B. White:** Methodology. **Ileana C. Miranda:** Investigation and validation. **Parirokh P. Awasthi:** Methodology. **Nasser K Altorki:** Resources. **Prajan Divakar:** Methodology. **Olivier Elemento:** Methodology. **Effie Apostolou:** Conceptualization and editing. **Giuseppe Giaccone:** Conceptualization, Funding acquisition; Supervision.

**Publisher's Disclaimer:** This is a PDF file of an unedited manuscript that has been accepted for publication. As a service to our customers we are providing this early version of the manuscript. The manuscript will undergo copyediting, typesetting, and review of the resulting proof before it is published in its final form. Please note that during the production process errors may be discovered which could affect the content, and all legal disclaimers that apply to the journal pertain.

<sup>i</sup>Laboratory of Comparative Pathology, Memorial Sloan Kettering Cancer Center, Weill Cornell Medicine, and The Rockefeller University, New York, NY 10065, USA

<sup>j</sup>Frederick National Laboratory for Cancer Research, Laboratory Animal Sciences, Mouse Modeling & Cryopreservation, National Cancer Institute, Frederick, MD 21701, USA

<sup>k</sup>Department of Cardiothoracic Surgery, Weill Cornell Medicine, New York Presbyterian Hospital, New York, NY10065, USA

<sup>l</sup>NanoString® Technologies Inc., Seattle, WA 98109, USA

## Abstract

**Introduction**—The pathogenesis of thymic epithelial tumors remains largely unknown. We previously identified *GTF2IL424H* as the most frequently recurrent mutation in thymic epithelial tumors. However, the precise role of this mutation in tumorigenesis of thymic epithelial cells is unclear.

**Methods**—To investigate the role of *GTF2IL424H* mutation in thymic epithelial cells *in vivo*, we generated and characterized a mouse model in which the *Gtf2i*L424H mutation was conditionally knocked-in in the *Foxn1*<sup>+</sup> thymic epithelial cells. Digital spatial profiling was performed on thymomas and normal thymic tissues with GeoMx-mouse whole transcriptome atlas. Immunohistochemistry staining (IHC) was performed using both mouse tissues and human thymic epithelial tumors.

**Results**—We observed that the *Gtf2i* mutation impairs development of thymic medulla and maturation of medullary thymic epithelial cells in young mice and causes tumor formation in the thymus of aged mice. Cell cycle related pathways, such as E2F targets and MYC targets are enriched in the tumor epithelial cells. GSVA analysis demonstrated that gene signatures of cortical thymic epithelial cells and thymic epithelial progenitor cells are also enriched in thymomas of the KI mice, which mirrors the human counterparts in the TCGA database. IHC results revealed similar expression pattern of epithelial cell markers between mouse and human thymomas.

**Conclusions**—We have developed and characterized a novel thymoma mouse model. This study improves knowledge of the molecular drivers in thymic epithelial cells and provides a tool for further study of the biology of thymic epithelial tumors and for development of novel therapies.

## Keywords

Mouse Model; Thymic Epithelial Tumors; GTF2I mutation

## Introduction

Thymic epithelial tumors (TETs), although rare, are the most common primary neoplasms of the mediastinum <sup>1</sup>. TETs are derived from thymic epithelial cells (TECs) in the medulla (mTECs) or cortex (cTECs) of the thymus. Histologically, TETs are divided into thymomas (A, AB, B1, B2, and B3 subtypes) and thymic carcinomas (TCs) <sup>2-5</sup>. Prognosis worsens progressively from type A thymoma to thymic carcinoma <sup>6,7</sup>. Thymomas are frequently associated with autoimmune disorders, myasthenia gravis (MG) being the most common. Surgery remains the cornerstone treatment for operable TETs, whereas the treatment of

advanced cases is mainly limited to chemotherapy, which is not curative, and palliative radiotherapy<sup>6,8</sup>. Several targeted therapies have been explored for the treatment of advanced TETs<sup>6</sup>, but their clinical benefit remains limited, due to lack of unique targetable alterations<sup>9,10</sup>. Pembrolizumab has shown promising activity, but is associated with an increased risk of autoimmune disorders<sup>11,12</sup>. Survival of advanced TETs ranges from 24% to 36% at 5 years for thymic carcinomas and thymomas, respectively<sup>13</sup>. Development of new therapies has been hindered by the lack of relevant disease models to help understand the molecular mechanisms of tumorigenesis.

We previously reported the identification of *GTF2I*L424H in TETs<sup>14</sup>, which have the lowest tumor mutation burden (TMB) among adult tumors<sup>1</sup>. This mutation was later confirmed by The Cancer Genome Atlas (TCGA) program, and is the most frequent mutation in TETs. This mutation is present in over 70% of types A and AB thymomas and less frequent in the more aggressive subtypes<sup>14</sup>. A recent study using laser capture microdissection and an enrichment strategy for next generation sequencing (NGS) was able to detect the *GTF2I* mutation also in 42% of type B thymomas<sup>15</sup>.

Recently, we showed that the *Gtf2i*L424H mutation confers survival advantage of the cells under metabolic stress and enhances tumorigenicity in immunocompromised mice, using immortalized mouse TEC cell lines<sup>16</sup>. In the current study, we generated a conditional *Gtf2i*L424H KI mouse model, in which *Gtf2i*L424H mutation is specifically expressed in *Foxn1*+ thymic epithelial cells. We observed defects in medulla development and maturation of medullary thymic epithelial cells in young mice and thymomas that histologically mirror human type B1/B2 thymomas in aged KI mice. Digital spatial profiling revealed similarity between thymomas from the KI mice and its counterpart in humans at transcriptional level. Cell cycle related pathways, such as E2F targets, MYC targets and G2M checkpoint, were activated in the thymoma lesions. In addition, gene signatures of cTEC and intertypical/thymic epithelial progenitor cells (TEPC) were highly enriched in the murine thymoma lesions, which mirrors the human *GTF2I* mutant TETs. This novel thymoma mouse model harboring *Gtf2i*L424H mutation represents an ideal tool for further studies of the biology of TETs and for the development of novel therapies.

## Material and Methods

### Generation of *Gtf2i* L424H knock-in mice.

The C57BL/6Ncr *Gtf2i*L424H floxed mice were generated by Mini-Gene strategy at Frederick National Laboratory for Cancer Research as illustrated in Fig 1C. A targeting vector was constructed, containing a 5' arm that is identical to the WT, a 3' arm that harbors a mutation on exon 15, and an insertion. The insertion is flanked by two loxp sites and consists of WT *Gtf2i* cDNA sequences (Exon15-34), a stop codon and a Neomycin resistance cassette. A targeted allele was obtained through homologous recombination. The mice carrying the targeted alleles were referred to as *Gtf2i*<sup>fl/wt</sup> or *Gtf2i*<sup>fl/fl</sup> mice. B6(cg)-*Foxn1*<sup>tm3(Cre)Nrm/J</sup> (*Foxn1*<sup>Cre/Cre</sup>) mice (stock 018448) were purchased from the Jackson Laboratory. *Gtf2i*<sup>fl/fl</sup> mice were crossed to *Foxn1*<sup>Cre/Cre</sup> mice to generate heterozygous KI mice (*Gtf2i*<sup>fl/wt</sup> *Foxn1*<sup>Cre/wt</sup>). The *Gtf2i*<sup>fl/wt</sup> *Foxn1*<sup>Cre/wt</sup> mice were further crossed to *Gtf2i*<sup>fl/wt</sup> *Foxn1*<sup>Cre/wt</sup> or *Gtf2i*<sup>fl/fl</sup> mice to generate homozygous KI, heterozygous KI

and control mice. The mice without KI allele(s) were used as control. Genotyping was done with genomic DNA from mouse tail tips or thymic tissues using specific primers (Supplementary Table 1). The *Gtf2i* L424H floxed mice have been deposited at Jackson laboratory (Stock 037506). Animal protocols were approved by the institutional animal use and care committee at Georgetown university and Weill Cornell Medicine.

### Pathological diagnosis.

The H&E and IHC staining slides were reviewed by two veterinary comparative pathologists, Dr. Ileana C Miranda and Dr. Sebastien Monette from The Laboratory of Comparative Pathology (LCP) and Genetically Modified Animal Phenotyping Service (GMAPS) of Weill Cornell Medicine, and 1 human pathologist, Dr. Alain C Borczuk, at Weill Cornell Medicine. The veterinary pathologists' interpretation was performed based on the International Harmonization of Nomenclature and Diagnostic Criteria for Lesions in Rats and Mice<sup>17,18</sup>.

### DSP sample preparation.

The FFPE tissue blocks were cut at 5µm thickness, and slides were subjected to in-situ mRNA hybridization, following the protocol recommended by Nanostring (Details are provided in Extended methods).

### Statistical analysis.

Statistical significance between two groups was calculated with a two-tailed Student's t test, and a value of  $p < 0.05$  was considered statistically significant. Statistical calculations were conducted using GraphPad Prism 9 software (GraphPad Software, San Diego, CA). Welch's One-way Analysis of Variance was performed on the gene expression means across samples from Thymus Cortical Epithelial, Thymus Medullary Epithelial, and Thymoma Epithelial. Tukey's HSD was performed to assess differences amongst groups. P-values from Gene Enrichment Analyses were adjusted according to the method of Benjamini Hochberg<sup>19</sup>.

## Results

### Generation of a novel thymoma mouse model with KI of the *Gtf2i* L424H mutation.

The *GTF2IL424H* mutation is present in 43% of patients with TETs (Fig. 1A). The frequency of *GTF2IL424H* mutation is highest in type A and AB thymomas (86% and 80% respectively), relatively lower in type B1, B2 and B3 thymomas (21%, 19% and 18%, respectively) and lowest in the TCs (4%) (Fig. 1B), consistent with our previous findings<sup>14</sup>. To investigate the role of *Gtf2i* L424H *in vivo*, we generated a KI mouse model, in which the expression of wild type (WT) *Gtf2i* is switched to mutant *Gtf2i* L424H, in the presence of Cre recombinase under the control of its own promoter (Fig. 1C). *Gtf2i* L424H-floxed mice were crossed with *Foxn1*-Cre mice to obtain *Gtf2i* L424H conditional KI mice, in which mutant *Gtf2i* L424H is expressed in *Foxn1* expressing TECs (Fig. 1C). Both heterozygous and homozygous KI mice were generated, and the genotypes of the mice were confirmed by genomic PCR using specific primers (Fig. 1D and Supplementary Table 1).

The heterozygous *Gtf2i*L424H KI mice were born at the expected Mendelian frequency and looked grossly normal. A small subgroup of mice showed abnormality in hair or skin. Two female mice displayed premature canities at 3-6 months of age (Supplementary Fig. 1A). Another three female mice were runt and developed inflammation and necrotic lesions on the ears, toes and tails (Supplementary Fig. 1C). Histological analysis revealed dermatitis, fibrosis, edema and hyperkeratosis whereas the tissues in the control were normal (Supplementary Fig. 1B vs C). *Foxn1* plays a role in skin development<sup>20</sup>, and the above lesions might be the result of the expression of *Gtf2i* mutation in the *Foxn1*<sup>+</sup> cells in the skin of affected mice. In addition, thymic lymphocytic apoptosis and lymphoid depletion were observed in 4 mice that were euthanized or died at 9-12 months. As shown in Supplementary Table 2, we also generated 24 homozygous KI mice, of which 15 died within 1 month and 3 died between 1-2 months. Only 6 mice survived more than 2.5 months and they were smaller than the age matched control littermates (Supplementary Fig. 1D). As the *GTF2I* mutation is heterozygous in human TETs<sup>14</sup>, heterozygous mice can better mimic pathogenesis in humans. Here, we focused further analysis on the heterozygous KI mice.

### ***Gtf2i* L424H mutation impairs development of the thymic medulla.**

We initially examined the heterozygous KI mice at age of 5 weeks. The medulla of KI mice was disorganized and appeared as scattered islands (Fig. 2B and B'), whereas the control medulla displayed sheets-like structures (Fig. 2A and A'). The percentage of total medullary areas was lower in the KI thymus than in the control thymus (Fig. 2E). The mean area of each medullary island in a thymus was also smaller in the KI mice than in the control mice (Fig. 2C-C' vs Fig. 2D-D', and Fig. 2F). The dominant cell populations were both Ck8<sup>+</sup> and Ck5+Ck8<sup>+</sup> cells in the KI medulla whereas the majority of cells were Ck5<sup>+</sup> in the control medulla (Fig. 2G and H). Ck5 and Ck8 are cellular markers for thymic epithelial cells in medulla and cortex, respectively<sup>21</sup>, and Ck5+Ck8<sup>+</sup> cells are thymic epithelial progenitor cells (TEPCs)<sup>21-23</sup>. High numbers of TEPCs have been described in mice with defective maturation of epithelial cells<sup>22</sup>. Therefore, the dominance of Ck5+Ck8<sup>+</sup> and Ck8<sup>+</sup> cells and reduction of Ck5<sup>+</sup> cells in the KI medulla indicate that *Gtf2i*L424H impairs the maturation of mTECs. Taken together, these results indicate that mutant *Gtf2i* impairs the development of medulla and maturation of mTECs.

### ***Gtf2i* L424H mutation induces murine thymomas that mirror the human counterparts in aged mice.**

The incidence of thymoma in humans is known to increase with age<sup>3</sup>. No thymoma formation was found in mice younger than 8 months by autoptic analysis of 15 mice aged 3-8 months. Of the 49 heterozygous KI mice older than 9 months, 21 developed thymoma, and all of them were female (Supplementary Table 3). Grossly, the thymic lobes were enlarged in the KI mice compared to control mice (Fig. 3A-A' and B-B'), and the ratio of thymus weight to body weight was significantly increased in the female KI mice (Supplementary Fig. 2A and B). The corticomedullary architecture was easily distinguishable by H&E and IHC staining in the thymus of control mice (Fig. 3C-C' and E-E'). B220<sup>+</sup> B cells were found in the corticomedullary and medullary regions whereas CD3<sup>+</sup> T cells were the dominant immune cell population across the whole thymus gland (Fig. 3G-G' and Supplementary Fig. 2C). In contrast, the enlarged thymus

of female KI mice displayed architectural distortion with loss of normal corticomedullary structures (Fig. 3D–D' and F–F'), with prominent epithelial cell population, mixed with abundant lymphocytic infiltrates (Fig. 3F–F' and H–H' and Supplementary Fig. 2D). The infiltrates are composed of CD3+ T cells and B220+ B cells, and the B cells frequently formed follicular like structures (Fig. 3H–H' and Supplementary Fig. 2D). These findings were interpreted as consistent with thymoma, epithelial subtype, according to rodent pathology diagnostic criteria<sup>17,18</sup>, by two veterinary comparative pathologists (I.C.M and S.M). The diagnosis of thymoma was further confirmed, and morphological features were found to be compatible with human type B1 thymoma with focal B2 lesions by a human pathologist (A.C.B.) (Supplementary Fig. 2H–K). In addition, frequent presence of multifocal hemorrhage and increased vascular density and diameter of vascular structures were found in the thymoma of KI mice compared to the thymus of control mice (Fig. 3I–I' and J–J'). Enrichment of epithelial cells was also found in the thymus of male KI mice, where a diagnosis of epithelial hyperplasia and epithelial cysts was made (Supplementary Fig. 2E). B cell follicular hyperplasia and hemorrhage were also found in those lesions (Supplementary Fig. 2F and G).

To characterize molecular features of the mouse thymomas, we performed digital spatial profiling on FFPE thymomas and normal thymic tissues with GeoMx-mouse whole transcriptome atlas (WTA), which covers more than 18,000 protein-coding genes<sup>24</sup>. As shown in Supplementary Fig. 3A, the epithelial cells, T cells and B cells were labeled by Pan-CK, CD3 and B220 antibodies, respectively. Based on the expression of these markers, regions of interest (ROIs) were selected for further sequencing by a board-certified pathologist (A.C.B.). 82 ROIs were available for downstream analysis (Supplementary Fig. 3B–E). Differentially expressed genes (DEGs) were identified by comparing thymoma epithelial ROIs to either medullary or cortical epithelial ROIs (Fig. 3K and Supplementary Fig. 4A and B). Gene Set Enrichment Analysis (GSEA)<sup>25</sup> revealed 113 positively and 4 negatively enriched transcription factor targets (TFT) gene sets (Supplementary Table 4)<sup>26</sup>. Interestingly, 8 out of the 10 top gene sets were related to E2F (Fig. 3 L # and M), indicating a prominent role of E2F regulated gene sets in thymoma epithelial cells. GSEA also identified 21 positively and 5 negatively enriched hallmark gene sets (Supplementary Table 5). The gene sets with highest enrichment scores were MYC\_targets\_V1, E2F\_targets and G2M checkpoint (Fig.3N, Supplementary Fig. 4C \* and Supplementary Fig. 4D–E, and Supplementary Table 5), which were also the top enriched pathways in DEGs of thymoma vs cortical epithelial cells (Supplementary Fig. 4F \* and G–I and Supplementary Table 6). E2F pathway was recently identified as the differentially activated pathway in human type B1 and B2 thymomas<sup>27</sup>, and the positive enrichment of E2F targets in the mouse type B1/B2 like thymomas resembles its human counterpart. Moreover, the negatively enriched hallmark gene sets in the mouse thymomas, including Interferon gamma response, Interferon alpha response, Inflammatory response, TNFA signaling via NFKB (Fig. 3O–R, Supplementary Fig. 4C, and Supplementary Table 5), were previously reported as the differentially repressed pathways in human type B1 and B2 thymomas<sup>27</sup>. In summary, thymomas in *Gtf2i* mutation KI mice resemble the human type B1/B2 thymomas at the transcriptional level.

### Heterogenous enrichment of cell cycle related gene sets in thymomas.

To determine the enriched pathways in each epithelial cell ROI, we performed Gene Set Variation Assay (GSVA)<sup>28</sup> analysis with the Hallmark gene sets (Fig. 4A). Consistent with the GSEA results, “MYC\_targets\_V1”, “E2F\_targets” and “G2M\_checkpoint” gene sets were highly enriched in most thymoma epithelial ROIs (Fig. 4A \*). The enrichment in thymoma ROIs was statistically significant when compared to either medullary (Fig. 4B) or cortical epithelial ROIs (Fig. 4C). GSVA analysis with TFT gene sets also confirmed the enrichment of E2F or MYC mediated targets in most thymoma ROIs (Supplementary Fig. 5A \*). The expression levels of the target genes were compared among representative ROIs from thymoma, medulla, and cortex (Fig. 4D–H). Expression levels of *Birc5*, *Top2a*, *Mki67* and *Mcm* family members were higher in thymoma ROIs than medullary or cortical ROIs (Fig. 4G and H), which is consistent with the enrichment of MYC and E2F pathways in the corresponding ROIs. IHC staining identified more E2f1+ cells in the tumor lesions than in the cortical area of the normal thymic tissues (Fig. 4K and N). Interestingly, the medullary area contained similar number of E2f1+ cells compared to thymoma lesions (Fig. 4K and N). However, expression levels of E2F targets were much higher in the thymoma than in the medullary epithelial ROIs (Fig. 4Q–R”), suggesting different activation status of E2F targets between thymoma and medullary epithelial cells. In addition, we observed significantly higher number of Mki67+ cells and c-Myc+ cells in the thymoma than in the medulla (Fig. 4L vs 4O and 4M vs 4P), which is consistent with the activation of MYC\_targets in the thymoma ROIs (Fig.4 A–C).

In addition, GSVA analysis also revealed enrichment of other pathways in thymoma ROIs, such as PI3K-Akt-mTOR signaling and Adipogenesis (Fig. 4 A #, B and C). Expression level of genes involved in PI3K-Akt-mTOR signaling and Adipogenesis pathways was also upregulated in thymoma ROIs compared to that in medullary or cortical ROIs (Fig. 4 I and J). The enrichment of PI3K-Akt-mTOR signaling and Adipogenesis pathways in this thymoma model is in line with our previous findings of PI3K as a potential target in TET cell lines harboring *PIK3R2* or *PIK3CA* mutations<sup>29</sup>, and altered lipid biosynthesis found in *Gtf2i* mutant KI cell lines<sup>16</sup>.

### Cellular composition in thymoma lesions.

To investigate the composition of epithelial cells in thymoma lesions, we performed GSVA analysis with gene signatures for mTEC, cTEC, intertypical TEC and proliferating TEC from existing single cell RNAseq data (Supplementary Table 7)<sup>30</sup>. Interestingly, cTEC gene signature was highly enriched in all thymoma ROIs. Intertypical TEC and mTEC gene signatures were also enriched in thymoma ROIs, with the exception of ROI-G10, G12 and H02 (Supplementary Fig. 5B). To verify the enrichment pattern of TEC signatures, we further performed GSVA analysis on 4 novel gene signatures for thymic epithelial subgroups (Supplementary Table 8)<sup>31</sup>. All thymoma epithelial ROIs showed enrichment in signature 3 (cTEC) (Supplementary Fig. 5C). The majority of thymoma ROIs also showed enrichment in signature 1&2 (Progenitor cells)<sup>31</sup>. Intertypical TEC signature consists of genes associated with progenitor like TEC<sup>lo</sup> phenotype<sup>30</sup>. Therefore, the cells that display high enrichment in signature 1&2 or intertypical TECs are potential TEPCs. In summary, these results suggest that thymomas are composed of heterogenous epithelial cells which

express genes associated with cTEC and TEPCs (Fig. 5A and Supplementary Fig. 5D). To investigate whether these signatures are present in human thymomas, we performed GSVA analysis with human TET samples from the TCGA database and showed that the human TETs can be stratified by these signatures. The human TETs with the *GTF2I* L424H mutation showed significantly higher enrichments in cTEC and intertypical TEC signatures, compared to the *GTF2I*WT tumors (Fig. 5E), which mirrors thymomas in our *Gtf2i*L424H KI mouse model. To further confirm the presence of heterogeneous epithelial cells in the thymoma lesions, we performed IHC staining with antibodies targeting Ck8/Ck18 and Ck5, which are cTEC and mTEC markers, respectively. Co-expression of cTEC and mTEC markers was observed in progenitor cells in the thymus<sup>21–23</sup>. In the normal mouse thymus, the Ck5+ and Ck8/18+ cells were mainly found in medulla and cortex, respectively (Fig. 5B). However, the thymoma lesions contain both Ck5+ and Ck8/Ck18+ cells (Fig. 5C–D'). Cells in some tumor areas appear to be positive for both Ck5 and Ck8/Ck18 (Fig. 5D–D', red line circled area). To confirm whether the heterogeneous cellular feature of epithelial cells is present in human thymomas, we performed IHC with CK5 and CK8 antibodies using tissue microarrays (TMAs) of human TETs. Interestingly, most TET cases are positive for both CK5 and CK8 (Fig. 5F–G'). There are more cases containing higher percentage of CK8+ and CK5+ cells in type A and type AB thymomas than other histological subtypes (Fig. 5H–I). These results indicate that the mouse thymoma lesions and the human thymomas share similar cellular features.

## Discussion

The lack of clinically relevant models has been a major roadblock to understanding the molecular features of TETs and to the development of novel therapies. TETs are rare spontaneous tumors in commonly used mouse strains<sup>18,32</sup>. Thymoma mouse models induced by carcinogens or polyoma virus have been reported<sup>33,34</sup>, but it is unclear whether these tumors recapitulate molecular features of human TETs. MYC, SV40 T-antigen, and E2F2 transgenic mouse models also develop thymomas<sup>35–37</sup>. However, these models have limited clinical relevance, since no amplification or mutations were identified in *MYC* and *E2F2* genes in human TETs (<https://www.cbioportal.org>). Here, we generated and characterized a conditional KI mouse model harboring a *Gtf2i*L424H mutation in the thymic epithelial cells, which developed thymomas. By whole transcriptomic profiling, we identified activated pathways and uncovered the gene signatures of cTEC and TEPC in the thymomas from the KI mice (Supplementary Fig. 6). We were the first to identify the *GTF2I* L424H as a recurrent mutation in human TETs in 2014, which was later confirmed by TCGA and other groups<sup>15,38</sup>. The TMB in TETs is the lowest among adult tumor types<sup>1</sup>, and the *GTF2I* mutation is more likely a driver mutation rather than a passenger mutation given that the *GTF2I* mutation is most frequently detected mutation and occasionally the only mutation detected by whole exome sequencing. The phenotype of our KI mouse model demonstrates that the *Gtf2i*L424H mutation is sufficient to induce tumorigenesis in the thymus.

MYC targets, E2F targets and G2M checkpoint gene sets were highly enriched in most thymoma lesions. MYC regulates genes associated with G2M checkpoint<sup>39</sup>, and can interact with E2F1 in regulating cell proliferation and apoptosis<sup>40,41</sup>. E2f1 expression

alone appeared to be insufficient to induce proliferation in normal medullary cells, since E2f1 expression was found in most cells in the medulla where cells expressing Myc and Mki67 were fewer (Fig. 4K–P). One possible explanation is that E2f1 activation rather than expression alone is required for cell proliferation in the thymus. The Retinoblastoma protein (Rb) regulates activation of E2F1<sup>42</sup>, and c-Myc can mediate activation of E2F in both Rb dependent and Rb independent manners<sup>43,44</sup>. It is therefore plausible that c-Myc interacts or activates E2f1 to induce cell proliferation in the thymus, since in fact c-Myc is a regulator of fetal thymus development and controls thymus size in mice<sup>45</sup>. Also, c-Myc overexpression driven by thy1 resulted in thymomas in transgenic mice<sup>35</sup>. c-Myc therefore appears to play a critical role for development and tumorigenesis in the thymus. Further studies to investigate whether *Gtf2i* mutation directly regulates c-Myc expression and E2f1 activation are needed.

Intriguingly, most thymoma lesions showed high enrichment in gene signatures of cTEC and TEPC (Fig. 5A, Supplementary Fig. 5B and D), which resembles the enrichment of such signatures in *GTF2I* mutant human TETs (Fig. 5E). In addition, we also observed increased cTEC and TEPC populations in the thymic tissues isolated from 5 weeks old KI mice (Fig. 2), suggesting cTEC and TEPC could be the cell of origin of *Gtf2i* mutant thymomas. Altogether, these results indicate that the thymoma cells are potentially derived from cTEC and TEPC cells and activation of cell cycle related pathways, such as Myc and E2f mediated targets, initiates the tumorigenesis in the *Gtf2i* mutant thymus.

Here, we demonstrated that *Gtf2i* L424H mutation in mouse thymus induces thymomas that histologically mirror human type B1/B2 thymomas. Although *GTF2I* mutations are seen in about 40% of type B thymomas by enriched NGS<sup>15</sup>, type A and AB have a much higher frequency of this mutation. It is not clear why our KI model displayed morphology resembling B1 and B2, but not other subtypes. One possibility is that other recurrent mutations in TETs may contribute to the histological subtypes of human TETs. It is noteworthy that one female heterozygous KI mouse developed epithelial hyperplasia with lymphoid deletion in the thymus. It is undetermined whether the hyperplastic lesion can further develop into tumors without enriched lymphoid components, which may mimic the histology of type A or AB thymomas in humans. Furthermore, we only detected thymomas in female mice, and observed thymic hyperplasia in the male KI mice. It is possible that sex hormone-mediated pathways may affect the tumor formation in the thymus of KI mice. The frequency of thymomas in humans is slightly higher in males than females (0.16 vs 0.13 per 100,000 person-years)<sup>46</sup>. There are however differences in animal strains that develop thymomas. In rats, the incidence of spontaneous thymoma is higher in female than male Wistar Hannover (WH) rats in two separate studies (15% vs 5% or 5.93% vs 2.67%)<sup>47,48</sup>, however, it was slightly lower in female than male F344/N rats (0.14% vs 0.18%)<sup>48</sup>.

In conclusion, we generated the first thymoma mouse model harboring a *Gtf2i* L424H mutation in the thymic epithelial cells. Through this unique mouse model, we characterized the transcriptomic profiles of thymomas, identified the activated pathways and uncovered the gene signatures of cTEC and TEPC in the thymomas (Supplementary Fig. 6). This KI mouse model provides a system for investigating the detailed molecular mechanism of TETs and for developing novel therapies in the future.

## Supplementary Material

Refer to Web version on PubMed Central for supplementary material.

## Acknowledgments

We thank Dr. Lewis C. Cantley for his suggestions on the project. We thank Dr. Thomas Boehm for insightful discussions. We thank Dr. Nancy Manley for her suggestion on the development of thymic medulla. We thank the comparative pathologist, Dr. Sebastien Monette from LCP (P30 CA008748), who made the diagnosis on thymic lesions of the KI mice. We also thank Dr. David Goldstein (NCI), Dr. ML Avantaggiati, Dr. Y Wang for their advice on the project. We also thank Taotao Zhang, Bing He and Leticia Dizon from TRP at Weill Cornell Medicine and Maria S. Jiao from LCP at MSK for supports on histological analyses.

### Funding:

This Work was supported by Intramural Research Program of the National Institutes of Health and the National Cancer Institute, ZIA BC 011304.

### Competing Interest Statement:

O.E. is supported by Janssen, J&J, Astra-Zeneca, Volastra and Eli Lilly research grants. He is scientific advisor and equity holder in Freenome, Owkin, Volastra Therapeutics and One Three Biotech and a paid scientific advisor to Pionyr Therapeutics and Champions Oncology. P.D. is an employee and stockholder at Nanostring Technologies Inc. J.B.W. is a compensated consultant for SpringWorks Therapeutics. NCI-Frederick is accredited by AAALAC International and follows the Public Health Service Policy for the Care and Use of Laboratory Animals. Animal care was provided in accordance with the procedures outlined in the "Guide for Care and Use of Laboratory Animals (National Research Council; 1996; National Academy Press; Washington, D.C.).

## References

- Marx A, Chan JKC, Chalabreysse L, et al. The 2021 WHO Classification of Tumors of the Thymus and Mediastinum: What Is New in Thymic Epithelial, Germ Cell, and Mesenchymal Tumors? *J Thorac Oncol* 17:200–213, 2022 [PubMed: 34695605]
- Travis WD, Brambilla E, Muller-Hermelink HK, et al. Pathology and genetics: Tumors of the lung, pleura, thymus and heart. , in Kleihues P, Sobin LH (eds): World Health Organization Classification of Tumours. Lyon, France, IARC Press, 2004, pp 145–247
- Engels EA: Epidemiology of thymoma and associated malignancies. *J Thorac Oncol* 5:S260–5, 2010 [PubMed: 20859116]
- Anderson G, Jenkinson EJ, Rodewald HR: A roadmap for thymic epithelial cell development. *Eur J Immunol* 39:1694–9, 2009 [PubMed: 19582736]
- Strobel P, Hohenberger P, Marx A: Thymoma and thymic carcinoma: molecular pathology and targeted therapy. *J Thorac Oncol* 5:S286–90, 2010 [PubMed: 20859121]
- Kelly RJ, Petrini I, Rajan A, et al. Thymic malignancies: from clinical management to targeted therapies. *J Clin Oncol* 29:4820–7, 2011 [PubMed: 22105817]
- Okumura M, Ohta M, Tateyama H, et al. The World Health Organization histologic classification system reflects the oncologic behavior of thymoma: a clinical study of 273 patients. *Cancer* 94:624–32, 2002 [PubMed: 11857293]
- Conforti F, Pala L, Giaccone G, et al. Thymic epithelial tumors: From biology to treatment. *Cancer Treat Rev* 86:102014, 2020 [PubMed: 32272379]
- Thomas A, Rajan A, Berman A, et al. Sunitinib in patients with chemotherapy-refractory thymoma and thymic carcinoma: an open-label phase 2 trial. *Lancet Oncol* 16:177–86, 2015 [PubMed: 25592632]
- Giaccone G, Rajan A, Berman A, et al. Phase II study of belinostat in patients with recurrent or refractory advanced thymic epithelial tumors. *J Clin Oncol* 29:2052–9, 2011 [PubMed: 21502553]
- Giaccone G, Kim C, Thompson J, et al. Pembrolizumab in patients with thymic carcinoma: a single-arm, single-centre, phase 2 study. *Lancet Oncol* 19:347–355, 2018 [PubMed: 29395863]

12. Cho J, Kim HS, Ku BM, et al. Pembrolizumab for Patients With Refractory or Relapsed Thymic Epithelial Tumor: An Open-Label Phase II Trial. *J Clin Oncol* 37:2162–2170, 2019 [PubMed: 29906252]
13. Kondo K, Monden Y: Therapy for thymic epithelial tumors: a clinical study of 1,320 patients from Japan. *Ann Thorac Surg* 76:878–84; discussion 884–5, 2003 [PubMed: 12963221]
14. Petrini I, Meltzer PS, Kim IK, et al. A specific missense mutation in GTF2I occurs at high frequency in thymic epithelial tumors. *Nat Genet* 46:844–9, 2014 [PubMed: 24974848]
15. Higuchi R, Goto T, Hirotsu Y, et al. Primary Driver Mutations in GTF2I Specific to the Development of Thymomas. *Cancers (Basel)* 12, 2020 [PubMed: 32718075]
16. Kim IK, Rao G, Zhao X, et al. Mutant GTF2I induces cell transformation and metabolic alterations in thymic epithelial cells. *Cell Death Differ* 27:2263–2279, 2020 [PubMed: 32034314]
17. Willard-Mack CL, Elmore SA, Hall WC, et al. Nonproliferative and Proliferative Lesions of the Rat and Mouse Hematolymphoid System. *Toxicol Pathol* 47:665–783, 2019 [PubMed: 31526133]
18. Rehg JE: Mouse Hematolymphoid Neoplasms, in John P. Sundberg PV, and Ward Jerrold M.. (ed): *Pathology of Genetically Engineered and Other Mutant Mice* (ed First Edition), John Wiley & Sons, Inc., 2022
19. Benjamini Y, Hochberg Y: Controlling the False Discovery Rate - a Practical and Powerful Approach to Multiple Testing. *Journal of the Royal Statistical Society Series B-Statistical Methodology* 57:289–300, 1995
20. Bukowska J, Kopcewicz M, Walenzik K, et al. Foxn1 in Skin Development, Homeostasis and Wound Healing. *Int J Mol Sci* 19, 2018 [PubMed: 30577572]
21. Lee EN, Park JK, Lee JR, et al. Characterization of the expression of cytokeratins 5, 8, and 14 in mouse thymic epithelial cells during thymus regeneration following acute thymic involution. *Anat Cell Biol* 44:14–24, 2011 [PubMed: 21519545]
22. Popa I, Zubkova I, Medvedovic M, et al. Regeneration of the adult thymus is preceded by the expansion of K5+K8+ epithelial cell progenitors and by increased expression of Trp63, cMyc and Tcf3 transcription factors in the thymic stroma. *Int Immunol* 19:1249–60, 2007 [PubMed: 17823311]
23. Sun X, Xu J, Lu H, et al. Directed differentiation of human embryonic stem cells into thymic epithelial progenitor-like cells reconstitutes the thymic microenvironment in vivo. *Cell Stem Cell* 13:230–6, 2013 [PubMed: 23910085]
24. Bergholtz H, Carter JM, Cesano A, et al. Best Practices for Spatial Profiling for Breast Cancer Research with the GeoMx((R)) Digital Spatial Profiler. *Cancers (Basel)* 13, 2021 [PubMed: 35008178]
25. Gennady KV Sukhov, Nikolay Budin, Boris Shpak, Maxim N. Artyomov; Alexey Sergushichev: Fast gene set enrichment analysis. *bioRxiv*, 2021
26. Subramanian A, Tamayo P, Mootha VK, et al. Gene set enrichment analysis: a knowledge-based approach for interpreting genome-wide expression profiles. *Proc Natl Acad Sci U S A* 102:15545–50, 2005 [PubMed: 16199517]
27. Benitez JC, Job B, de Montpreville VT, et al. Cancer activation pathways of thymic epithelial tumors (TETs) by targeted gene expression analysis. *Journal of Clinical Oncology* 39, 2021
28. Hanzelmann S, Castelo R, Guinney J: GSEA: gene set variation analysis for microarray and RNA-seq data. *BMC Bioinformatics* 14:7, 2013 [PubMed: 23323831]
29. Alberobello AT, Wang Y, Beerkens FJ, et al. PI3K as a Potential Therapeutic Target in Thymic Epithelial Tumors. *J Thorac Oncol* 11:1345–1356, 2016 [PubMed: 27117832]
30. Baran-Gale J, Morgan MD, Maio S, et al. Ageing compromises mouse thymus function and remodels epithelial cell differentiation. *Elife* 9, 2020
31. Nusser A, Sagar, Swann JB, et al. Developmental dynamics of two bipotent thymic epithelial progenitor types. *Nature* 606:165–171, 2022 [PubMed: 35614226]
32. Pearse G: Histopathology of the thymus. *Toxicol Pathol* 34:515–47, 2006 [PubMed: 17067942]
33. Stutman O, Yunis EJ, Good RA: Carcinogen-induced tumors of the thymus. I. Restoration of neonatally thymectomized mice with a functional thymoma. *J Natl Cancer Inst* 41:1431–52, 1968 [PubMed: 5728344]

34. Hoot GP, Kettman JR: Primary polyoma virus-induced murine thymic epithelial tumors. A tumor model of thymus physiology. *Am J Pathol* 135:679–95, 1989 [PubMed: 2552813]
35. Spanopoulou E, Early A, Elliott J, et al. Complex lymphoid and epithelial thymic tumours in Thy1-myc transgenic mice. *Nature* 342:185–9, 1989 [PubMed: 2572968]
36. Lee SS, Park WY, Chi JG, et al. Thymic epithelial tumor progression in an SV40T transgenic mouse model. Cortical thymoma-thymic carcinoma sequence. *Virchows Arch* 432:33–42, 1998 [PubMed: 9463585]
37. Scheijen B, Bronk M, van der Meer T, et al. High incidence of thymic epithelial tumors in E2F2 transgenic mice. *J Biol Chem* 279:10476–83, 2004 [PubMed: 14684733]
38. Radovich M, Pickering CR, Felau I, et al. The Integrated Genomic Landscape of Thymic Epithelial Tumors. *Cancer Cell* 33:244–258 e10, 2018 [PubMed: 29438696]
39. Yang Y, Xue K, Li Z, et al. c-Myc regulates the CDK1/cyclin B1 dependent G2/M cell cycle progression by histone H4 acetylation in Raji cells. *Int J Mol Med* 41:3366–3378, 2018 [PubMed: 29512702]
40. Matsumura I, Tanaka H, Kanakura Y: E2F1 and c-Myc in cell growth and death. *Cell Cycle* 2:333–8, 2003 [PubMed: 12851485]
41. Ladu S, Calvisi DF, Conner EA, et al. E2F1 inhibits c-Myc-driven apoptosis via PIK3CA/Akt/mTOR and COX-2 in a mouse model of human liver cancer. *Gastroenterology* 135:1322–32, 2008 [PubMed: 18722373]
42. Trimarchi JM, Lees JA: Sibling rivalry in the E2F family. *Nat Rev Mol Cell Biol* 3:11–20, 2002 [PubMed: 11823794]
43. Leung JY, Ehmann GL, Giangrande PH, et al. A role for Myc in facilitating transcription activation by E2F1. *Oncogene* 27:4172–9, 2008 [PubMed: 18345030]
44. Dong P, Maddali MV, Srimani JK, et al. Division of labour between Myc and G1 cyclins in cell cycle commitment and pace control. *Nat Commun* 5:4750, 2014 [PubMed: 25175461]
45. Cowan JE, Malin J, Zhao Y, et al. Myc controls a distinct transcriptional program in fetal thymic epithelial cells that determines thymus growth. *Nat Commun* 10:5498, 2019 [PubMed: 31792212]
46. Engels EA, Pfeiffer RM: Malignant thymoma in the United States: demographic patterns in incidence and associations with subsequent malignancies. *Int J Cancer* 105:546–51, 2003 [PubMed: 12712448]
47. Tomonari Y, Sato J, Kurotaki T, et al. Thymomas and Associated Hyperplastic Lesions in Wistar Hannover Rats. *Toxicol Pathol* 47:129–137, 2019 [PubMed: 30700236]
48. Moore RR, Nagai H, Miller RA, et al. Comparative Incidences and Biological Outcomes for Thymoma in Various Rat Strains in National Toxicology Program Studies. *Toxicol Pathol* 47:833–841, 2019 [PubMed: 31394971]

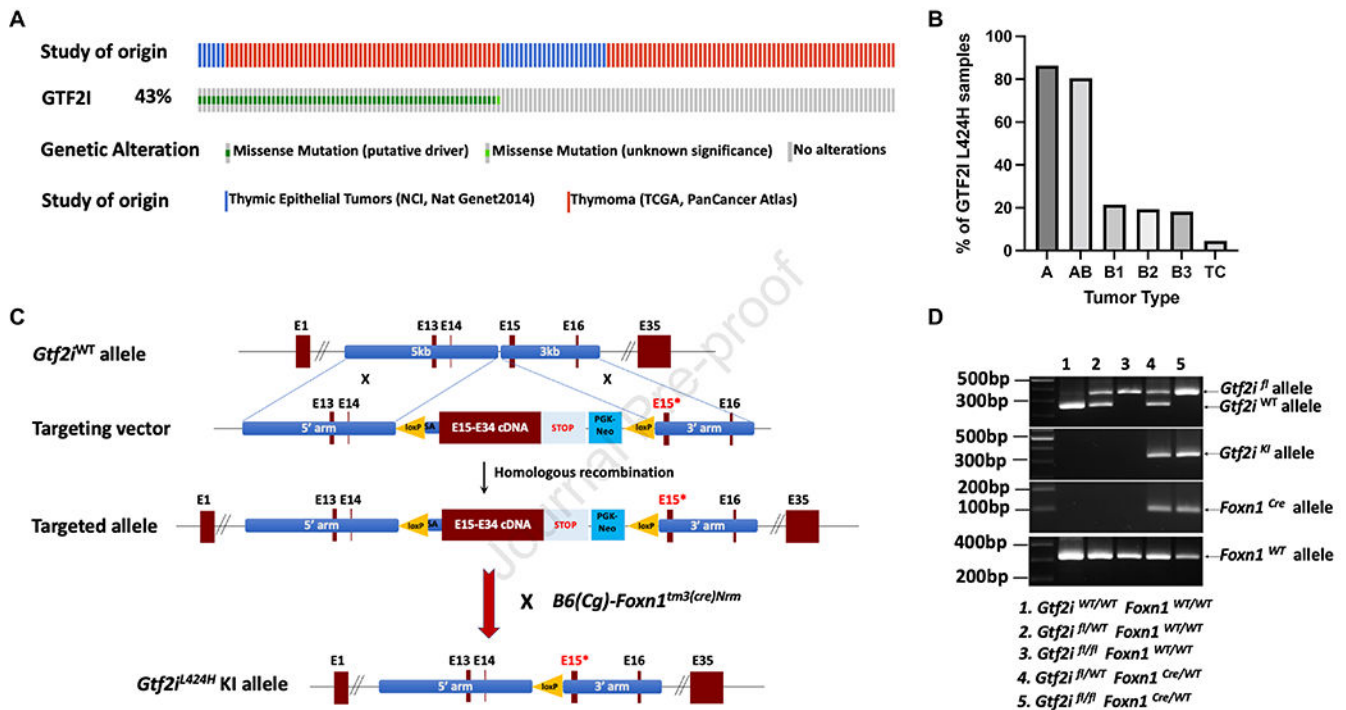


**Figure 1. Generation of a knock-in mouse model harboring the *Gtf2i* L424H mutation.**

**A.** Oncoprint image of patient samples with thymic epithelial tumors (TETs) from two patient cohorts, as indicated. The analysis shows that 43% of TETs harbor the *GTF2I*L424H mutation. **B.** Frequency of the *GTF2I*L424H mutation in each histologic subtype of TETs. The frequency of *GTF2I*L424H mutation is 86%, 80%, 21%, 19%, 18% and 4% in type A, AB, B1, B2, B3 thymomas, and thymic carcinomas (TCs), respectively, in the indicated patient cohorts. **C.** Schematic of strategy for generating *Gtf2i* targeted and knock-in (KI) alleles. The targeted (or floxed) allele contains a 5' arm, a 3' arm and an insertion between the 5' and 3' arms. The 5' arm of the targeted allele is identical to that of WT *Gtf2i*, whereas the 3' arm of the targeted allele harbors a mutation on Exon 15. The insertion is flanked by two loxp sites and consists of WT *Gtf2i* cDNA sequences (Exon15-34), a stop codon and a Neomycin resistance cassette. The mice carrying the targeted allele were crossed to B6(cg)-*Foxn1*<sup>tm3(cre)Nrm</sup> mice to generate conditional KI mice. **D.** Representative images of genomic PCR confirming the *Gtf2i* wt, *Gtf2i*-floxed, *Gtf2i*-KI, *Foxn1* wt and *Cre* alleles.

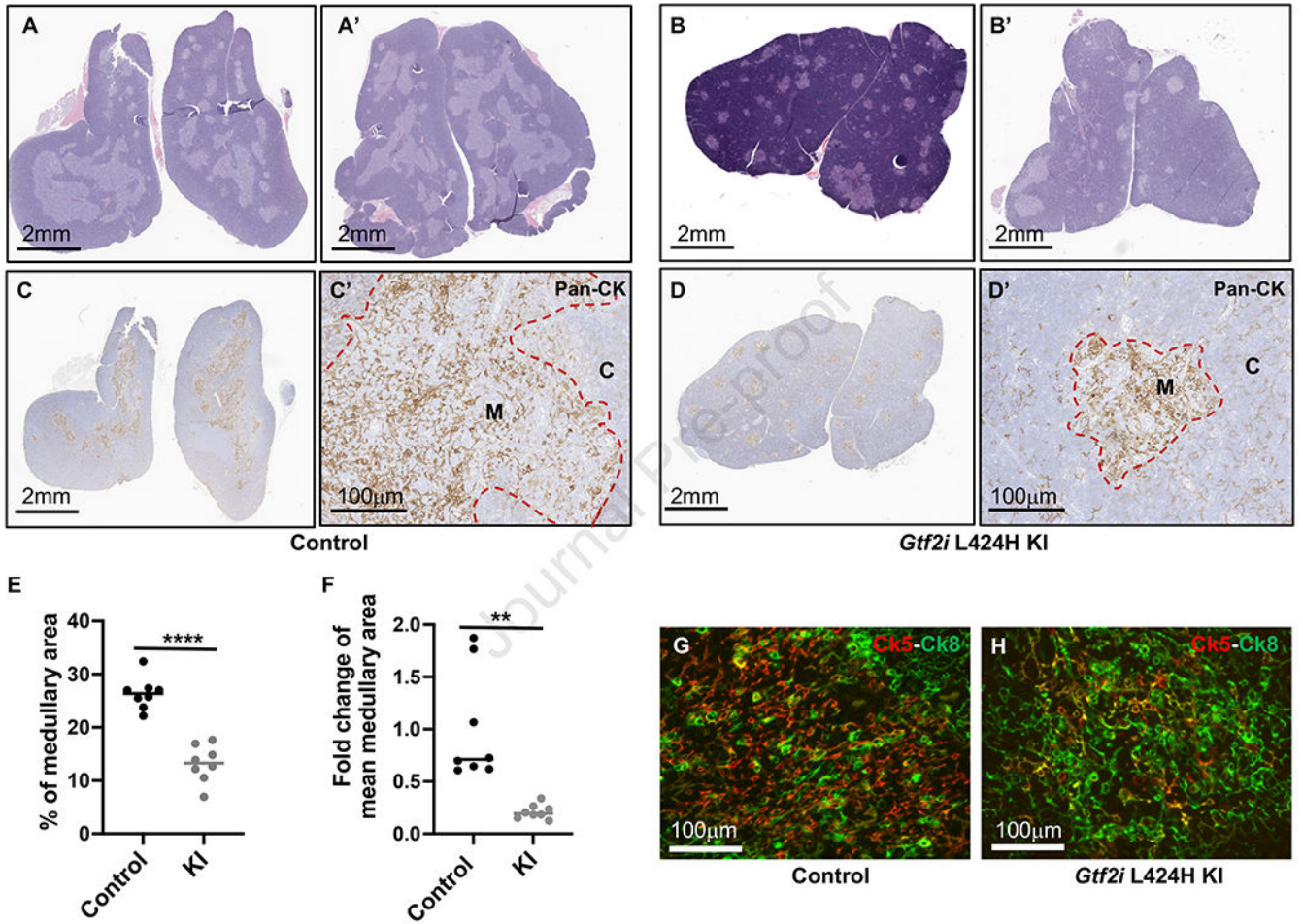


**Figure 2. *Gtf2i* L424H mutation impairs development of thymic medulla and maturation of medullary thymic epithelial cells.**

**A-D.** Representative images of H&E and IHC staining with thymic tissues isolated from control (A&C) and *Gtf2i* L424H KI (B&D) mice. A-A' & B-B'. H&E staining was performed on FFPE slides of thymic tissues from control and KI mice. C-C' & D-D'. IHC staining was performed using pan-cytokeratin antibody. M: medulla; C: cortex. Red dot line indicates the medullary area. Scale bar: 2mm or 100µm. **E.** Dot plot showing the percentage of medullary area in the thymic tissues of control and KI mice. The total area and medullary area were measured on the H&E staining images using image J. % of total medullary area was calculated as medullary area/total thymic area. 8 thymic tissues were included in each group. \*\*\*\*,  $p < 0.0001$ . **F.** Dot plot showing the fold change of mean medullary area in the control thymus compared to the KI thymus. The mean medullary area was calculated as total medullary area/number of medulla islands in a thymus. 8 thymic tissues were included in each group. \*\*,  $p < 0.01$ . **G-H.** Representative images of co-immunofluorescent staining with thymic tissues of control (G) and KI (H) mice. The thymic tissues were subjected to co-immunofluorescent (co-IF) staining with Ck5 (Red) and Ck8 (Green) antibodies. Scale bar: 100µm.

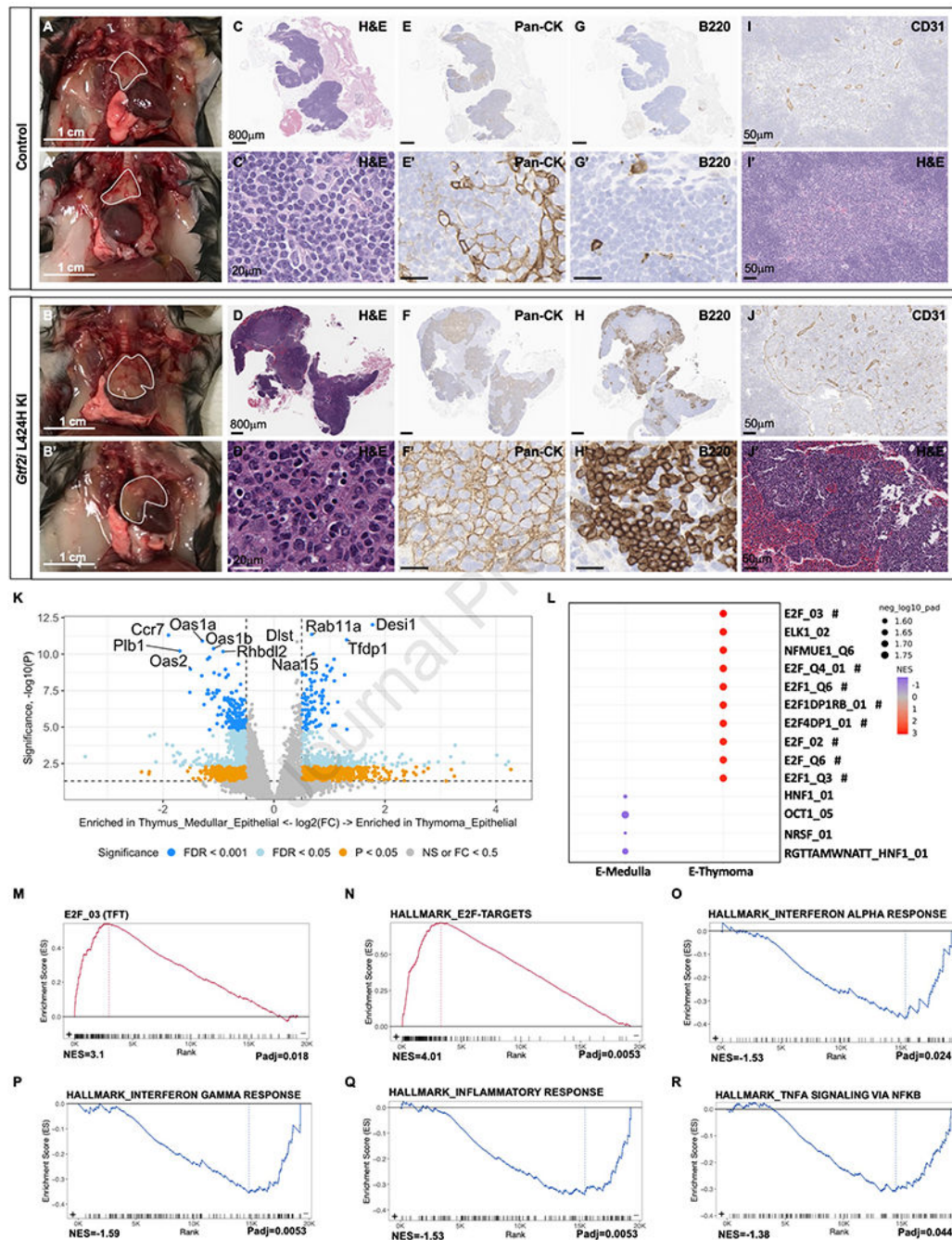


**Figure 3. *Gtf2i* L424H mutation induces murine thymomas that mirror the human counterparts in aged heterozygous KI mice.**

**A-B.** Representative images of thymic tissues from female control (A-A') and KI (B-B') mice. The thymic tissues are highlighted by the white circle. Scale bar: 1 cm. **C-D.** Representative images of H&E staining with thymic tissues from female control and KI mice. Scale bar: 800 $\mu$ m or 20 $\mu$ m. **E-H, I and J.** Representative images of IHC staining with thymic tissues from female control and KI mice. The IHC staining was performed using Pan-cytokeratin (E-E' and F-F'), B220 (G-G' and H-H') or CD31 (I and J) antibodies.

Scale bar: 800 $\mu$ m, 50 $\mu$ m or 20 $\mu$ m, as indicated. **I'&J'**, Representative images of H&E staining with thymic tissues from female control and KI mice, as indicated. Scale bar: 50 $\mu$ m. **K**. Volcano plot showing the differentially expressed genes (DEGs) between thymoma epithelial cells and medullary epithelial cells. **L**. Dot plot showing relative enrichment of TET pathways in thymoma epithelial and medullary epithelial cells. Top 10 positively enriched gene sets were selected based on the adjusted p-value and NES; 1 unknown gene set was removed from the top 10 list. Only 4 negatively enriched gene sets were significant. **M-R**. Representative GSEA enrichment plots showing that DEGs of thymoma epithelial cells vs medullary epithelial cells were positively Or negatively enriched in the gene sets, as indicated.

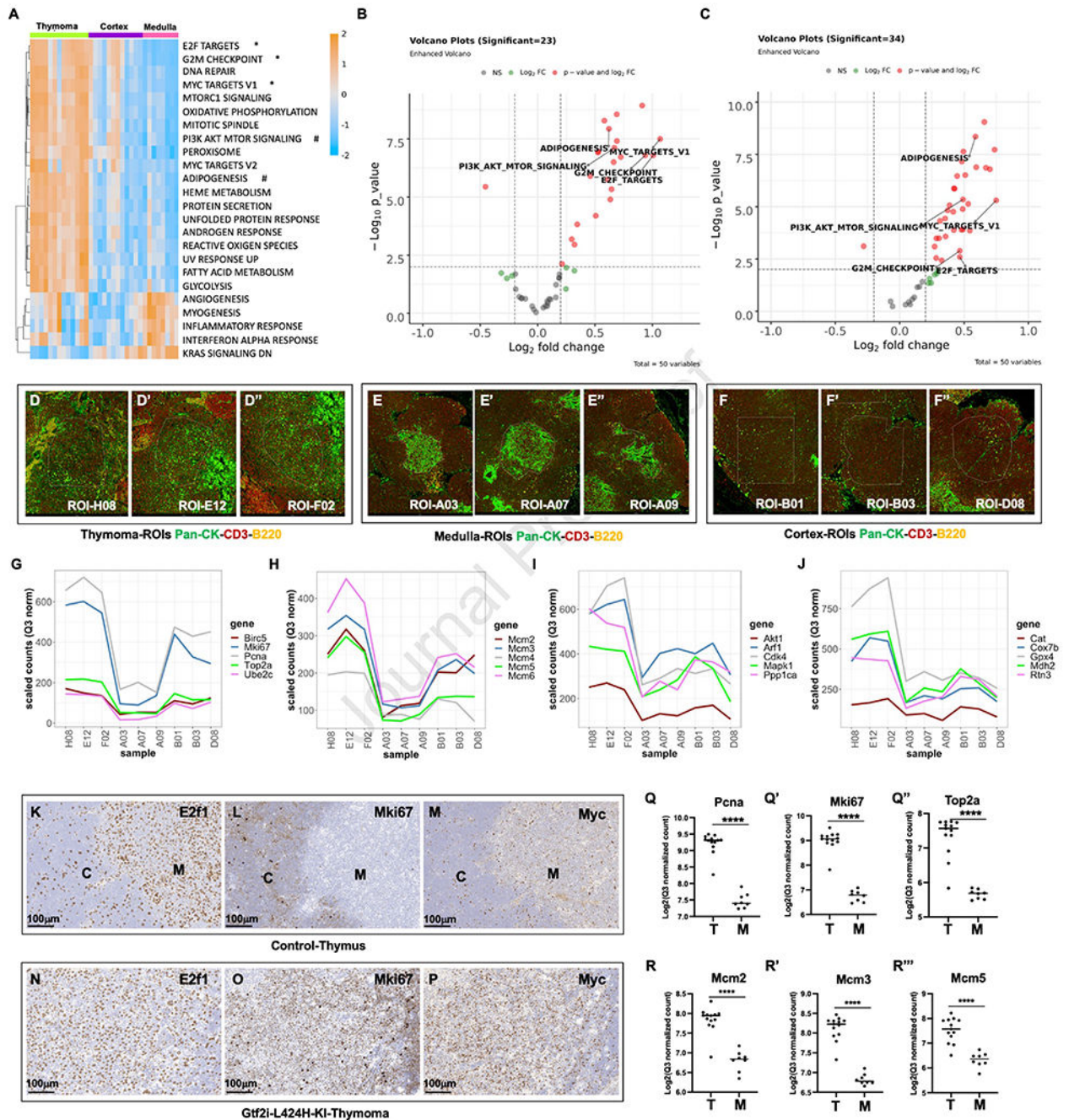


**Figure 4. Cell cycle related pathways are enriched in thymoma lesions.**

**A.** Heatmap of GSEA enrichment scores showing the enrichment of indicated pathways in each epithelial ROI from thymoma, normal cortex and medulla. \* and # represent highlighted gene sets in Fig.4B and 4C. **B-C.** Volcano plots showing the significant hallmark gene sets between thymoma vs medullary epithelial cells (B) or that of thymoma vs cortical epithelial cells (C). **D-F.** Triple staining images of representative ROIs from thymoma (D-D''), medulla (E-E'') and cortex (F-F''). Green, Pan-CK; red, CD3; yellow, B220. **G-H.** Line plots showing the expression level of genes from MYC\_TARGETS\_V1, E2F

TARGETS AND G2M CHECKPOINT in each ROI, as indicated. **I-J**. Line plots showing the expression level of genes from PI3K\_AKT\_MTOR (I) or ADIPOGENESIS (J) in each ROI, as indicated. **K-P**. Representative images of IHC staining with thymic tissues from control (K-M) and KI (N-P) mice. The IHC was performed using E2f1 (K and N), Mki67 (L and O), and c-Myc (M and P) antibodies. Scale bar: 100 $\mu$ m. **Q-R**. Log2 Q3 normalized expression of genes involved in cell cycle related pathways in thymoma and medullary epithelial ROIs.

Author Manuscript

Author Manuscript

Author Manuscript

Author Manuscript

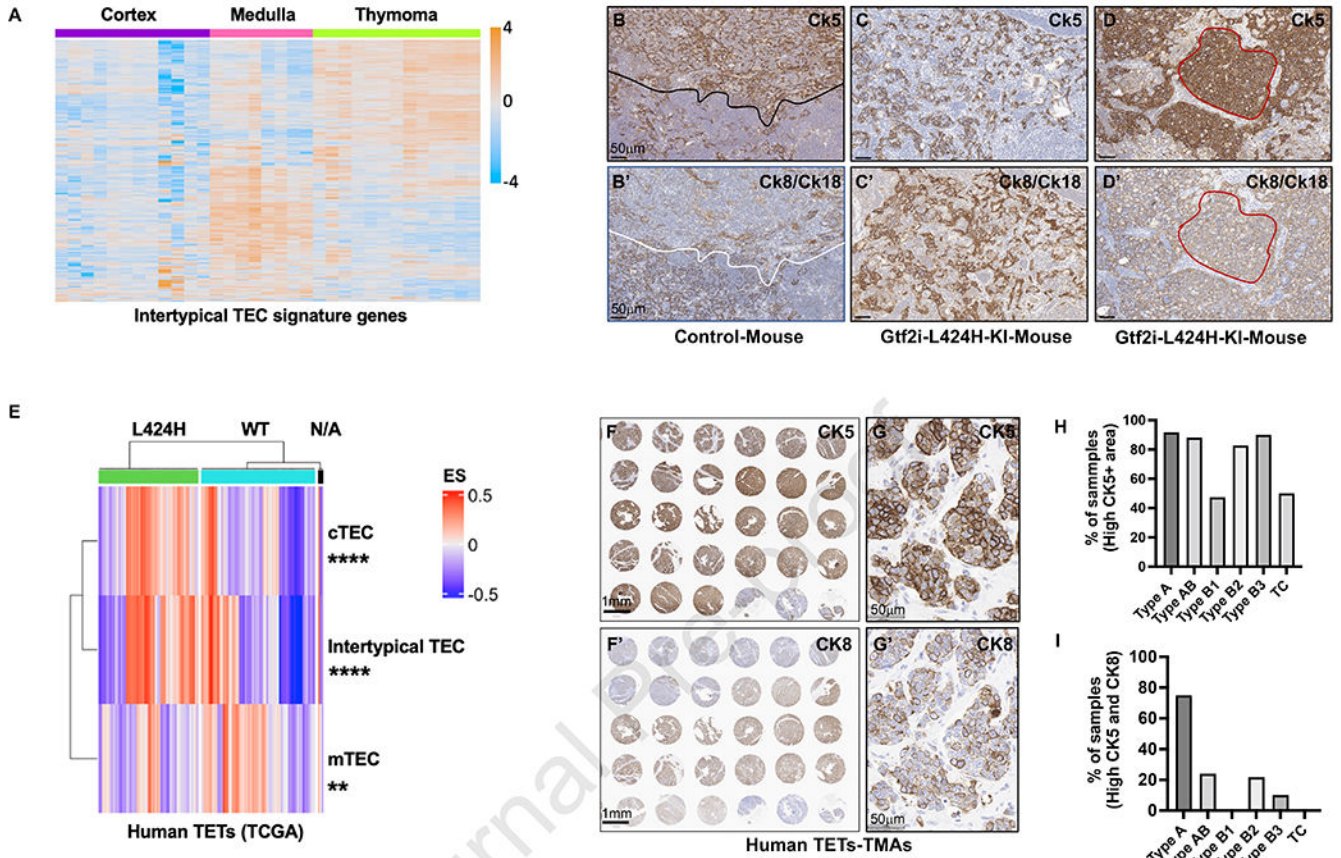


**Figure 5. Heterogeneous expression pattern of epithelial cell signatures in thymomas.**

**A.** Heatmap showing expression of intertypical signature genes in cortex, medulla and thymoma epithelial ROIs. **B-D.** Representative images of IHC staining with the thymic tissues from control (B) and KI (C-D) mice. The adjacent FFPE slides of thymic tissues were subjected to IHC staining with Ck5 (B, C and D) and Ck8/18 (B', C', and D') antibodies. Scale bar: 50µm. B. Thymic tissues from control mice. C-D. Thymoma tissues from KI mice, red circle, the area containing cells positive to both Ck5 and Ck8/18. **E.** Heatmap of GSV enrichment scores showing enrichment of cTEC, intertypical TEC and mTEC gene signatures in human TETs with/without *GTF2I* mutation. **F-G.** Representative images of IHC staining with the tissue microarrays (TMA) of human TETs. TMA was generated with human TET samples and adjacent sections of TMAs were subjected to IHC staining with CK5 (F-G) and CK8 (F'-G') antibodies. Scale bar: 1mm 50µm as indicated. **H-I.** % of samples containing relatively high percentage of CK5+ (H) or both CK5+ and CK8+ (I) areas in each histological TET subtype, based on the IHC staining with TMAs of human TETs.